Available online at www.sciencedirect.com
ScienceDirect
International Journal of Solids and Structures 44 (2007) 7988–8005
INTERNATIONAL JOURNAL OF SOLIDS AND STRUCTURES
www.elsevier.com/locate/ijsolstr

Elastic field of an isotropic matrix with a nanoscale elliptical inhomogeneity

L. Tian, R.K.N.D. Rajapakse *

Department of Mechanical Engineering, The University of British Columbia, Vancouver, BC, Canada V6T 1Z4

Received 9 June 2006; received in revised form 2 May 2007
Available online 2 June 2007

Abstract

In traditional continuum mechanics, the effect of surface energy is ignored as it is small compared to the bulk energy. For nanoscale materials and structures, however, the surface effects become significant due to the high surface/volume ratio. In this paper, two-dimensional elastic field of a nanoscale elliptical inhomogeneity embedded in an infinite matrix under arbitrary remote loading and a uniform eigenstrain in the inhomogeneity is investigated. The Gurtin–Murdoch surface/interface elasticity model is applied to take into account the surface/interface stress effects. By using the complex variable technique of Muskhelishvili, the analytic potential functions are obtained in the form of an infinite series. Selected numerical results are presented to study the size-dependency of the elastic field and the effects of surface elastic moduli and residual surface stress. It is found that the elastic field of an elliptic inhomogeneity under uniform eigenstrain is no longer uniform when the interfacial stress effects are taken into account.

Keywords: Surface stress; Nanoscale inhomogeneity; Stress concentration; Size-dependency

1. Introduction

Nanomaterials are categorized as those which have structured components with at least one dimension less than 100 nm. They can be further categorized into one-dimensional nanoscale (thin films, layers and surfaces), two-dimensional nanoscale (nanotubes and nanowires) and three-dimensional nanoscale (nanoparticles, quatum dots and dendrimers) materials. An important application of nanoparticles and nanotubes is in advanced composite materials. Composites based on nanomaterials can be tailored to have unique mechanical, electronic and optical properties (Kuzumake et al., 1998; Cui and Lieber, 2001; Naganuma and Kagawa, 2002).

As the dimension of a material or structure approaches the nanoscale, the properties and elastic field can be size-dependent. For example, Wong et al. (1997) and Poncharal et al. (1999) experimentally investigated the elastic bending of SiC nanobeams and carbon nanotubes, respectively, and showed that the bending modulus changes as the diameter of the beam or tubes changes. The classical continuum theory, however, does not

* Corresponding author. Tel.: +1 6048220497; fax: +1 6048220944.
E-mail address: rajapakse@mech.ubc.ca (R.K.N.D. Rajapakse).

0020-7683/$ - see front matter © 2007 Elsevier Ltd. All rights reserved.
doi:10.1016/j.ijsolstr.2007.05.019

admit an intrinsic size, and does not show size-dependent behaviour. To understand the behavior of nanomaterials and nanoscale structures, various approaches have been proposed including atomistic simulation methods. The reason for the size-dependent behaviour at nanoscale is the presence of free surfaces, and the fraction of energy stored in the surfaces becomes comparable with that in bulk for nanoscale structures. Mechanics of nanoscale objects can therefore be understood by incorporating the effects of surface and interfacial energies (Miller and Shenoy, 2000). The surface stress theory formulated by Gibbs (1906), on the basis of thermodynamics of solid surfaces, takes into consideration the effects of surface and interfacial energies. Gurtin and Murdoch (1975), Murdoch (1976) and Gurtin et al. (1998) developed a general theoretical framework for a continuum with surface stresses and proposed a linearized surface stress–strain constitutive relation. The surface domain is assumed to be very thin and has different elastic moduli from the bulk, and the surface adheres to the bulk without slipping. Several other researchers have contributed to further development of the surface stress theory (e.g., Cahn and Larché, 1982; Cammarata, 1994; Nix and Gao, 1998).

Gurtin and Murdoch (1978), Povstenko (1993), Cammarata (1997) and Miller and Shenoy (2000) have applied the surface stress theory to examine several issues involving nanoscale problems. Sharma et al. (2003), Sharma and Ganti (2004) and Duan et al. (2005) studied the size-dependent elastic state of nanoinhomogeneities, Eshelby's tensor of nanoinclusions and effective bulk and shear moduli of a solid containing nanoinhomogeneities, respectively, by applying the Gurtin–Murdoch model. Tian and Rajapakse (2007) obtained a closed-form analytical solution for a nanoscale circular inhomogeneity in an infinite matrix under arbitrary remote loading based on the Gurtin–Murdoch model.

The solution for a nanoscale elliptical inhomogeneity in an infinite matrix is a very important fundamental problem in nanoscale solid mechanics as it is practically more useful than the solution for the idealized case of a circular or spherical inhomogeneity. This paper is therefore concerned with the derivation of the two-dimensional elastic field of an infinite matrix with an elliptical inhomogeneity due to remote loading or an eigenstrain in the inhomogeneity. Muskhelishvili (1963) provided a powerful complex variable approach to analyze two-dimensional inhomogeneity problems in classical elasticity. A review of the application of Muskhelishvili's approach for inhomogeneity problems in classical elasticity is beyond the scope of this paper. The authors use the Gurtin–Murdoch model and Muskhelishvili's complex potential method to study the two-dimensional size-dependent elastic field of a nanoscale elliptical inhomogeneity in an infinite elastic matrix. The derivation of the solution is presented in the next section followed by numerical results for selected cases.

2. Problem formulation

Consider an infinite elastic matrix, with a single nanoscale elliptical inhomogeneity. The matrix is subjected to far-field loading as shown in Fig. 1 and a uniform eigenstrain is prescribed in the inhomogeneity. The matrix and inhomogeneity are linear elastic, homogeneous and isotropic with Lamé constants λ_M, μ_M and

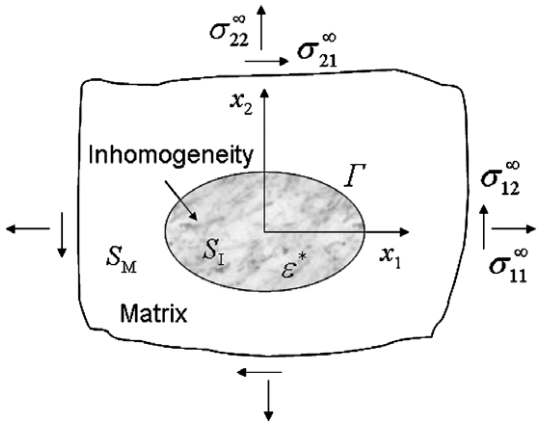

Fig. 1. Nanoscale elliptical inhomogeneity in an infinite matrix.

λ_I, μ_I, respectively. Note that subscripts M and I are used to identify quantities associated with the matrix and inhomogeneity, respectively. The matrix occupies a region denoted by S_M, and the inhomogeneity, with its center at the origin of the coordinate system, occupies a region denoted by S_I. The ellipse Γ represents the matrix–inhomogeneity interface.

For plane problems, the displacement and stress components in Cartesian coordinates (x_1, x_2, x_3) can be expressed in terms of two analytic functions $\phi(z)$ and $\psi(z)$ as (Muskhelishvili, 1963)

$$2\mu(u_1 + \mathrm{i}u_2) = \kappa\phi(z) - z\overline{\phi'(z)} - \overline{\psi(z)}, \tag{1}$$

$$\sigma_{11} + \sigma_{22} = 2\left[\phi'(z) + \overline{\phi'(z)}\right], \tag{2}$$

$$\sigma_{22} - \sigma_{11} + 2\mathrm{i}\sigma_{12} = 2[\bar{z}\phi''(z) + \psi'(z)], \tag{3}$$

where u_i and σ_{ij} are displacement and stress components, respectively, $z = x_1 + \mathrm{i}x_2$ is the complex coordinate variable, μ and v are the shear modulus and Poisson's ratio, respectively, and $\kappa = 3 - 4v$ for plane stain and $(3 - v)/(1 + v)$ for plane stress. Overbar in Eqs. (1)–(3) represents a complex conjugate and the prime denotes differentiation with respect to the argument.

At the interface Γ, the boundary displacements and tractions can be written in the normal-tangential coordinates (n, t) as

$$2\mu(u_n + \mathrm{i}u_t) = \left[\kappa\phi(z) - z\overline{\phi'(z)} - \overline{\psi(z)}\right]\mathrm{e}^{-\mathrm{i}\alpha}, \tag{4}$$

$$\sigma_{nn} - \mathrm{i}\sigma_{nt} = \phi'(z) + \overline{\phi'(z)} - [\bar{z}\phi''(z) + \psi'(z)]\mathrm{e}^{2\mathrm{i}\alpha}, \tag{5}$$

where t is the unit tangent, and n is the outward unit normal at the interface which in complex form is equal to $\mathrm{e}^{\mathrm{i}\alpha}$ (where α is the angle between the normal direction n and the positive x_1-axis).

Assume that the inhomogeneity is perfectly bonded to the matrix, then the displacements are continuous at the interface

$$(u_n + \mathrm{i}u_t)_M = (u_n + \mathrm{i}u_t)_I + (u_n + \mathrm{i}u_t)^*_I, \quad \text{on } \Gamma, \tag{6}$$

where the last term is the displacement induced by the prescribed uniform dilatational eigenstrain ε^*, i.e., $\varepsilon^*_{11} = \varepsilon^*_{22} = \varepsilon^*$, and

$$(u_n + \mathrm{i}u_t)^*_I = z\varepsilon^*\mathrm{e}^{-\mathrm{i}\alpha}, \quad \text{on } \Gamma. \tag{7}$$

The following field equations and constitutive relations can be established for an isotropic material based on the theory proposed by Gurtin and Murdoch (1975) and Gurtin et al. (1998):

In the bulk (matrix and inhomogeneity)

$$\sigma^B_{ij,j} = 0, \quad \sigma^B_{ij} = \lambda\delta_{ij}\varepsilon_{kk} + 2\mu\varepsilon_{ij}. \tag{8}$$

On the surface/interface Γ

$$[\![\sigma^B_{\beta\alpha}n_\beta]\!] + \sigma^S_{\beta\alpha,\beta} = 0, \tag{9}$$

$$[\![\sigma^B_{ji}n_in_j]\!] = \sigma^S_{\alpha\beta}k_{\alpha\beta}, \tag{10}$$

$$\sigma^S_{\beta\alpha} = \tau^0\delta_{\beta\alpha} + 2(\mu^S - \tau^0)\varepsilon_{\beta\alpha} + (\lambda^S + \tau^0)\varepsilon_{\gamma\gamma}\delta_{\beta\alpha}, \tag{11}$$

where superscripts B and S are used to denote the quantities corresponding to bulk (matrix and inhomogeneity) and surface/interface of inhomogeneity; σ_{ij} and ε_{ij} denote stress and strain, respectively; λ and μ are Lamé constants; δ_{ij} is the Kronecker delta; n_i is the normal vector on the surface/interface; λ^S and μ^S are the surface Lamé constants; τ^0 is the residual surface stress under unstrained conditions; $k_{\alpha\beta}$ is the curvature tensor of the surface or interface and $[\![*]\!] = (*)_M - (*)_I$ denotes the jump across the matrix–inhomogeneity interface.

The surface stress tensor is a 2D quantity and the strain normal to the surface is excluded in Eq. (11). Thus, the Greek indices take the value of 1 or 2, while Latin subscripts adopt values 1 though 3.

In the (n, t, x_3) coordinates [x_3 is the direction perpendicular to the (n, t)-plane], the equilibrium Eqs. (9) and (10) can be written as

On the surface/interface Γ

$$\text{In } t\text{-direction}: [\![\sigma^{B}_{nt}]\!] + \frac{\partial \sigma^{S}_{tt}}{\partial t} + \frac{\partial \sigma^{S}_{3t}}{\partial x_3} = 0, \tag{12}$$

$$\text{In } x_3\text{-direction}: [\![\sigma^{B}_{n3}]\!] + \frac{\partial \sigma^{S}_{33}}{\partial x_3} + \frac{\partial \sigma^{S}_{t3}}{\partial t} = 0, \tag{13}$$

$$\text{In } n\text{-direction}: [\![\sigma^{B}_{nn}]\!] = \frac{\sigma^{S}_{tt}}{R_0}, \tag{14}$$

where R_0 is the radius of curvature.

For plane problems, $\sigma^{B}_{n3} = \sigma^{S}_{3t} = \sigma^{S}_{t3} = 0$ and the derivatives with respect to x_3 are zero. Thus Eq. (13) is automatically satisfied. Eqs. (12) and (14) can be expressed in the following complex variable form:

$$[\![\sigma^{B}_{nn} - \mathrm{i}\sigma^{B}_{nt}]\!] = \frac{\sigma^{S}_{tt}}{R_0} + \mathrm{i}\frac{\partial \sigma^{S}_{tt}}{\partial t}. \tag{15}$$

The left-hand side of Eq. (15) can be obtained from Eq. (5). For the right-hand side, the surface normal stress in the tangential direction is

$$\sigma^{S}_{tt} = \tau^0 + 2(\mu^{S} - \tau^0)\varepsilon_{tt} + (\lambda^{S} + \tau^0)(\varepsilon_{33} + \varepsilon_{tt}), \quad \text{on } \Gamma. \tag{16}$$

Special attention is required when calculating the strain ε_{33} at the interface, because the strain at either side of the interface can be different even though the displacement is assumed to be continuous. Thus, the interface has two interfacial stresses associated with it. Here, the authors take the average of the two interfacial stresses as this is consistent with the case of a circular inhomogeneity in which the interface stress is continuous for plane strain problems and only one interface stress or the average of the two is used in Eq. (15) (Sharma and Ganti, 2004). In the case of a hole, there is only one interface stress, or more exactly, the surface stress, and only this stress appears in the right-hand side of Eq. (15).

Tangential elastic stain at the surface, ε_{tt}, can be obtained from the following equations:

$$\varepsilon_{tt} + \varepsilon_{nn} = \varepsilon_{11} + \varepsilon_{22} = \frac{1}{Q}\left(\phi'(z) + \overline{\phi'(z)}\right), \quad \text{on } \Gamma, \tag{17}$$

$$\varepsilon_{tt} - \varepsilon_{nn} + 2\mathrm{i}\varepsilon_{nt} = (\varepsilon_{22} - \varepsilon_{11} + 2\mathrm{i}\varepsilon_{12})\mathrm{e}^{2\mathrm{i}\alpha} = \frac{1}{\mu}[\bar{z}\phi''(z) + \psi'(z)]\mathrm{e}^{2\mathrm{i}\alpha}, \quad \text{on } \Gamma. \tag{18}$$

Here, $Q = \lambda + \mu$ for plane strain and $\mu(3\lambda + 2\mu)/(\lambda + 2\mu)$ for plane stress. Therefore,

$$\varepsilon_{tt} = \frac{1}{2Q}\left(\phi'(z) + \overline{\phi'(z)}\right) + \frac{1}{4\mu}[\bar{z}\phi''(z) + \psi'(z)]\mathrm{e}^{2\mathrm{i}\alpha} + \frac{1}{4\mu}\left[z\overline{\phi''(z)} + \overline{\psi'(z)}\right]\mathrm{e}^{-2\mathrm{i}\alpha}. \tag{19}$$

In the matrix, the elastic strain ε_{tt} is also the actual strain. In the inhomogeneity, due to the eigenstrain effect, $(\varepsilon_{tt})_{\mathrm{I}} = (\varepsilon_{tt})^{\mathrm{e}}_{\mathrm{I}} + \varepsilon^*$, where $(\varepsilon_{tt})^{\mathrm{e}}_{\mathrm{I}}$ is the elastic strain in the inhomogeneity which can be obtained form Eq. (19).

For the other strain in Eq. (15), $\varepsilon_{33} = 0$ for plane strain in both matrix and inhomogeneity, and for plane stress, $(\varepsilon_{33})_{\mathrm{M}} = v_{\mathrm{M}}(\varepsilon_{nn} + \varepsilon_{tt})^{\mathrm{e}}_{\mathrm{M}}/(v_{\mathrm{M}} - 1)$ in the matrix and $(\varepsilon_{33})_{\mathrm{I}} = v_{\mathrm{I}}[(\varepsilon_{nn} + \varepsilon_{tt})^{\mathrm{e}}_{\mathrm{I}} + 2\varepsilon^*]/(v_{\mathrm{I}} - 1)$ in the inhomogeneity. Here $(\varepsilon_{nn} + \varepsilon_{tt})^{\mathrm{e}}_{\mathrm{M}}$ and $(\varepsilon_{nn} + \varepsilon_{tt})^{\mathrm{e}}_{\mathrm{I}}$ are the elastic strains in the matrix and inhomogeneity, respectively, which can be obtained by using Eq. (17).

Following Muskhelishvili (1963) and England (1971), introduce the following mapping function to simplify the geometry of the problem (Fig. 2).

$$z = m(\xi) = R\left(\xi + \frac{m}{\xi}\right), \quad \sqrt{m}\xi = \frac{z}{l}\left\{1 + \left[1 - \left(\frac{l}{z}\right)^2\right]^{1/2}\right\}, \quad \xi = \zeta + \mathrm{i}\eta = r\mathrm{e}^{\mathrm{i}\theta}. \tag{20}$$

Here,

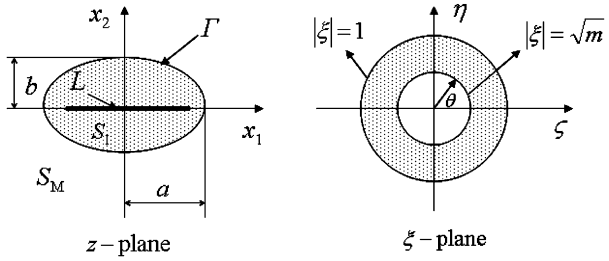

Fig. 2. Conformal mapping from z-plane to ξ-plane.

$$R=\frac{a+b}{2},\quad m=\frac{1-a/b}{1+a/b}\quad\text{and}\quad l=\sqrt{a^2-b^2}, \tag{21}$$

where a and b are the semi-axes of the ellipse and $0\leqslant m\leqslant 1$.

When $m=0$, the ellipse becomes a circle and in the limit $m=1$ it becomes a crack. The mapping function transforms the region S_M into the exterior region of a unit circle ($|\xi|=1$) and region S_I into an annular region between the unit circle and a circle of radius $|\xi|=\sqrt{m}$. Here the region S_I is imagined to be cut along the line $L=\{(x_1,0):-l\leqslant x_1\leqslant l\}$ which is transformed into a circle with radius $|\xi|=\sqrt{m}$.

Assume that there are no singularity points in the region S_I, then $\phi_I(z)$ and $\psi_I(z)$ must be holomorphic in the region S_I and

$$\phi_I(z)=\phi_I(\bar{z}),\quad \psi_I(z)=\psi_I(\bar{z}),\quad z\in L. \tag{22}$$

Consequently, the conditions (22) ensure that $\phi_I(z)$ and $\psi_I(z)$ are analytic functions throughout the region S_I.

Now take $\phi(\xi)=\phi(m(\xi))$, and $\psi(\xi)=\psi(m(\xi))$ in the mapped ξ-plane. Therefore, the conditions (22) become

$$\phi_I(\xi)=\phi_I(\overline{\xi}),\quad \psi_I(\xi)=\psi_I(\overline{\xi}),\quad \forall\xi:|\xi|=\sqrt{m}. \tag{23}$$

The complex potentials $\phi_M(\xi)$, $\phi_I(\xi)$, $\psi_M(\xi)$ and $\psi_I(\xi)$ corresponding to the matrix and inhomogeneity are now expanded into the following Laurent series form:

$$\phi_M(\xi)=A\xi+\sum_{n=1}^{\infty}A_n\xi^{-n},\quad \psi_M(\xi)=B\xi+\sum_{n=1}^{\infty}B_n\xi^{-n}, \tag{24}$$

$$\phi_I(\xi)=\sum_{n=1}^{\infty}(E_n\xi^n+F_n\xi^{-n}),\quad \psi_I(\xi)=\sum_{n=1}^{\infty}(G_n\xi^n+H_n\xi^{-n}). \tag{25}$$

Note that the constant terms have been omitted in Eqs. (24) and (25) since they represent the rigid body displacements and have no effect on the stress distribution. A and B are given constants characterizing the remote stress field. In view of Eqs. (2) and (3),

$$\sigma_{11}^{\infty}+\sigma_{22}^{\infty}=\frac{2(A+\overline{A})}{R},\quad \sigma_{22}^{\infty}-\sigma_{11}^{\infty}+2\mathrm{i}\sigma_{12}^{\infty}=\frac{2B}{R}, \tag{26}$$

where σ_{11}^{∞}, σ_{22}^{∞} and σ_{12}^{∞} are the far-field stresses.

According to England (1971), the imaginary part of A is related to the rotation ω_{∞} at infinity and,

$$\omega_{\infty}=(1+\kappa)\mathrm{Im}(A)/2\mu. \tag{27}$$

In the current problem, the rotation is zero, so that,

$$A=\overline{A}. \tag{28}$$

Following Stagni (1991) and Shen et al. (2001), introduce an auxiliary functions $\Omega(\xi)$ and a new auxiliary function $\Theta(\xi)$ such that,

$$\Omega(\xi) = \overline{\frac{m(1/\bar{\xi})}{m'(\xi)}}\phi'(\xi) + \psi(\xi), \tag{29}$$

$$\Theta(\xi) = \Omega'(\xi)m'(\xi) - \phi'(\xi)\left[\overline{m(1/\bar{\xi})}\right]'. \tag{30}$$

The auxiliary functions $\Omega_M(\xi)$, $\Theta_M(\xi)$, $\Omega_I(\xi)$ and $\Theta_I(\xi)$ corresponding to the matrix and inhomogeneity can also be expanded into Laurent series as,

$$\Omega_M(\xi) = C\xi + C_0 + \sum_{n=1}^{\infty} C_n\xi^{-n}, \quad \Theta_M(\xi) = \left(D\xi + D_0 + \sum_{n=1}^{\infty} D_n\xi^{-n}\right)R, \tag{31}$$

$$\Omega_I(\xi) = L_0 + \sum_{n=1}^{\infty}(L_n\xi^n + M_n\xi^{-n}), \quad \Theta_I(\xi) = \left[O_0 + \sum_{n=1}^{\infty}(O_n\xi^n + P_n\xi^{-n})\right]R. \tag{32}$$

Eq. (31) combined with Eqs. (24), (29) and (30) leads to

$$C = mA + B, \quad C_0 = 0, \tag{33}$$
$$D = 0, \quad D_0 = B,$$
$$D_1 = 0, \quad D_2 = -Cm - C_1 + A + mA_1, \quad D_3 = -2C_2 + 2mA_2,$$
$$D_{n+3} = -(n+2)C_{n+2} + mnC_n + m(n+2)A_{n+2} - nA_n \quad (n = 1, 2, 3\ldots). \tag{34}$$

Eq. (32) combined with Eqs. (25) and (30) results in the following relations between the coefficients O_n, P_n and E_n, F_n, L_n and M_n.

$$O_0 = -3mL_3 + L_1 + 3E_3 - mE_1,$$
$$O_n = -(n+3)mL_{n+3} + (n+1)L_{n+1} + (n+3)E_{n+3} - (n+1)mE_{n+1} \quad (n = 1, 2, 3\ldots), \tag{35}$$
$$P_1 = -2mL_2 + 2E_2, \quad P_2 = -mL_1 - M_1 + E_1 + mF_1, \quad P_3 = -2M_2 + 2mF_2,$$
$$P_{n+3} = nmM_n - (n+2)M_{n+2} - nF_n + (n+2)mF_{n+2} \quad (n = 1, 2, 3\ldots). \tag{36}$$

Furthermore, Eq. (23) combined with Eqs. (25), (29) and (32) yields

$$F_n = m^nE_n, \quad H_n = m^nG_n, \quad M_n = m^nL_n + nm^{n-1}(1 - m^2)E_n. \tag{37}$$

Using Eqs. (4), (7), (29) and the continuity of displacements across the interface, Eq. (6), can be expressed as

$$\frac{1}{2\mu_M}\left[\kappa_M\phi_M(\xi) - \overline{\Omega_M(\xi)}\right] = \frac{1}{2\mu_I}\left[\kappa_I\phi_I(\xi) - \overline{\Omega_I(\xi)}\right] + m(\xi)\varepsilon^*. \tag{38}$$

Noting that $\xi = e^{i\theta}$ on the interface, substitute Eqs. (24), (25), (31) and (32) into Eq. (38) and equate the coefficients of $e^{in\theta}$ to obtain the following relations.

$$L_0 = 0, \quad \Lambda_3(\kappa_M A - \overline{C}_1) = \kappa_I E_1 - \overline{M}_1 + 2\mu_I R\varepsilon^*,$$
$$\Lambda_3(-\overline{C}_{n+1}) = \kappa_I E_{n+1} - \overline{M}_{n+1} \quad (n = 1, 2, 3, \ldots), \tag{39}$$
$$\Lambda_3(\kappa_M A_1 - \overline{C}) = \kappa_I F_1 - \overline{L}_1 + 2\mu_I Rm\varepsilon^*,$$
$$\Lambda_3\kappa_M A_{n+1} = \kappa_I F_{n+1} - \overline{L}_{n+1} \quad (n = 1, 2, 3, \ldots). \tag{40}$$

where $\Lambda_3 = \mu_I/\mu_M$.

To solve the present problem, it is required to obtain the coefficients including A_n, C_n, D_n, E_n, L_n, O_n and P_n. Once these are known, the other coefficients (B_n, F_n, H_n and M_n) can be determined. Based on the above analysis, D_n can be expressed in terms of A_n and C_n from Eq. (34); E_n and L_n can be expressed in terms of A_n and C_n from Eqs. (37), (39) and (40); O_n and P_n can be expressed in terms of E_n and L_n from Eqs. (35) to (37), and thus in terms of A_n and C_n. The only unknown coefficients are therefore A_n and C_n. Additional relations between the unknowns can be obtained from the interface equilibrium Eq. (15) by using the following procedure.

Following England (1971),

$$e^{2i\alpha}=\frac{\xi m'(\xi)}{\overline{\xi m'(\xi)}},\quad e^{i\alpha}=\frac{\xi m'(\xi)}{|\xi m'(\xi)|};\xi=e^{i\theta}\quad \text{on } \Gamma, \tag{41}$$

and the derivatives with respect to the tangential direction t can be expressed as,

$$\frac{\partial}{\partial t}=\frac{\partial}{\partial z}\frac{\partial z}{\partial t}+\frac{\partial}{\partial \bar{z}}\frac{\partial \bar{z}}{\partial t}=\frac{\partial}{\partial \xi}\frac{1}{\frac{\partial z}{\partial \xi}}\frac{\partial z}{\partial t}+\frac{\partial}{\partial \bar{\xi}}\frac{1}{\frac{\partial \bar{z}}{\partial \bar{\xi}}}\frac{\partial \bar{z}}{\partial t}, \tag{42}$$

$$\frac{\partial z}{\partial t}=ie^{i\alpha},\quad \frac{\partial \bar{z}}{\partial t}=-ie^{-i\alpha}. \tag{43}$$

In the ξ-plane, Eq. (5) becomes

$$\sigma_{nn}-i\sigma_{nt}=\frac{\phi'(\xi)}{m'(\xi)}+\frac{\overline{\phi'(\xi)}}{\overline{m'(\xi)}}-\left\{\left(\frac{\phi''(\xi)m'(\xi)-\phi'(\xi)m''(\xi)}{[m'(\xi)]^2}\right)\frac{\overline{m(\xi)}}{\overline{m'(\xi)}}+\frac{\psi'(\xi)}{\overline{m'(\xi)}}\right\}e^{2i\theta},\quad \text{on } \Gamma.$$

Multiplying the above expression by the (non-vanishing) factor $\overline{m'(\xi)}$, and eliminating $\psi'(\xi)$ by using Eq. (29), yields

$$\overline{m'(\xi)}[\sigma_{nn}-i\sigma_{nt}]=\overline{\phi'(\xi)}-e^{2i\theta}\Omega'(\xi). \tag{44}$$

The right-hand side of Eq. (15) can be written as

$$\frac{\sigma^S_{tt}}{R_0}+i\frac{\partial\sigma^S_{tt}}{\partial t}=\frac{\frac{1}{2}\left[(\sigma^S_{tt})_M+(\sigma^S_{tt})_I\right]}{R_0}+i\frac{\partial\left[\frac{1}{2}(\sigma^S_{tt})_M+\frac{1}{2}(\sigma^S_{tt})_I\right]}{\partial t}. \tag{45}$$

The two interface stresses are derived separately in Appendix A by substituting Eq. (16) into the above equation and multiplying the resulting expression by a factor $\frac{m'(\xi)\overline{m'(\xi)}/R}{m'(\xi)/R}$.

Consequently by combining Eqs. (24), (25), (31), (32), (44) and (A5), Eq. (15) becomes

$$\begin{aligned}&\sum\nolimits_{n=1}^{\infty}n(C_n-\overline{E}_n-M_n)e^{-i(n-1)\theta}+A-Ce^{2i\theta}-\sum_{n=1}^{\infty}n\left(\overline{A}_n-\overline{F}_n-L_n\right)e^{i(n+1)\theta}\\&=\frac{1}{m'(\xi)/R}\frac{1}{|m'(\xi)/R|^3}\Big[g_0+h_0+(g_1+h_1)e^{-i\theta}+(g_2+h_2)e^{i\theta}+(g_3+h_3)e^{-2i\theta}\\&\quad+(g_4+h_4)e^{2i\theta}+(g_5+h_5)e^{-3i\theta}+(g_6+h_6)e^{3i\theta}+h_7e^{-4i\theta}+h_8e^{4i\theta}\\&\quad+\sum_{n=1}^{\infty}S_ne^{i(n+3)\theta}+\sum_{n=1}^{\infty}T_ne^{-i(n+3)\theta}+\sum_{n=1}^{\infty}U_ne^{i(n+4)\theta}+\sum_{n=1}^{\infty}V_ne^{-i(n+4)\theta}\Big].\end{aligned} \tag{46}$$

The coefficients g_0, $g_n(n=1,2,\ldots,6)$, $h_n(n=1,2,\ldots,8)$, S_n, T_n, U_n and V_n are defined in Appendix A.

Next, employing a method similar to that used by Shen et al. (2000), $\frac{1}{|m'(\xi)/R|^3}$ can be expanded into an infinite series of the following form (see Appendix B).

$$\frac{1}{|m'(\xi)/R|^3}=\frac{1}{(1-m)^3}(1+b^*\sin^2\theta)^{-3/2},\quad b^*=\frac{4m}{(1-m)^2}, \tag{47}$$

$$\begin{aligned}\left(1+b^*\sin^2\theta\right)^{-3/2}&=I_0+\sum_{k=1}^{\infty}I_{2k}(e^{i2k\theta}+e^{-i2k\theta}),\\&\cong I_0+\sum_{k=1}^{J-1}I_{2k}(e^{i2k\theta}+e^{-i2k\theta})+I_{2J}\frac{e^{i2J\theta}+e^{-i2J\theta}-m(e^{i2(J-1)\theta}+e^{i2(1-J)\theta})}{(1-me^{2i\theta})(1-me^{-2i\theta})}.\end{aligned} \tag{48}$$

Eq. (48) can now be rewritten as

$$(1+b^*\sin^2\theta)^{-3/2}\cong\frac{1}{(1-me^{2i\theta})(1-me^{-2i\theta})}\left[f_0+\sum_{k=1}^{J}f_{2k}(e^{i2k\theta}+e^{-i2k\theta})\right], \tag{49}$$

where

$$f_0 = (1+m^2)I_0 - 2mI_2,$$
$$f_{2k} = (1+m^2)I_{2k} - mI_{2k-2} - mI_{2k+2} \quad (k = 1,2,\ldots,J-1),$$
$$f_{2J} = I_{2J} - mI_{2J-2}. \tag{50}$$

Take the denominator $(1-m\mathrm{e}^{2\mathrm{i}\theta})(1-m\mathrm{e}^{-2\mathrm{i}\theta})$ into the first term of the right-hand side of Eq. (46), i.e., $\frac{1}{m'(\xi)/R}$, and expand it into a power series of the following form (see Appendix B).

$$\frac{1}{m'(\xi)/R}\frac{1}{(1-m\mathrm{e}^{2\mathrm{i}\theta})(1-m\mathrm{e}^{-2\mathrm{i}\theta})} = \frac{1}{(1-m^2)^2}\left[\sum_{n=1}^{\infty} m^n \mathrm{e}^{\mathrm{i}2n\theta} + 1 + \sum_{n=1}^{\infty}(m^n + (1-m^2)nm^n)\mathrm{e}^{-\mathrm{i}2n\theta}\right]. \tag{51}$$

Thereafter, using Eqs. (47), (49) and (51), Eq. (46) becomes

$$\begin{aligned}
&\sum_{n=1}^{\infty} n(C_n - \overline{E}_n - M_n)\mathrm{e}^{-\mathrm{i}(n-1)\theta} + A - C\mathrm{e}^{2\mathrm{i}\theta} - \sum_{n=1}^{\infty} n(\overline{A}_n - \overline{F}_n - L_n)\mathrm{e}^{\mathrm{i}(n+1)\theta} \\
&= \frac{1}{(1-m)^3(1-m^2)^2}\left[\sum_{n=1}^{\infty} m^n \mathrm{e}^{\mathrm{i}2n\theta} + 1 + \sum_{n=1}^{\infty}(m^n + (1-m^2)nm^n)\mathrm{e}^{-\mathrm{i}2n\theta}\right]\left[f_0 + \sum_{k=1}^{J} f_{2k}(\mathrm{e}^{\mathrm{i}2k\theta} + \mathrm{e}^{-\mathrm{i}2k\theta})\right] \\
&\quad \times \Big[g_0 + h_0 + (g_1+h_1)\mathrm{e}^{-\mathrm{i}\theta} + (g_2+h_2)\mathrm{e}^{\mathrm{i}\theta} + (g_3+h_3)\mathrm{e}^{-2\mathrm{i}\theta} + (g_4+h_4)\mathrm{e}^{2\mathrm{i}\theta} \\
&\quad + (g_5+h_5)\mathrm{e}^{-3\mathrm{i}\theta} + (g_6+h_6)\mathrm{e}^{3\mathrm{i}\theta} + h_7\mathrm{e}^{-4\mathrm{i}\theta} + h_8\mathrm{e}^{4\mathrm{i}\theta} \\
&\quad + \sum_{n=1}^{\infty} S_n\mathrm{e}^{\mathrm{i}(n+3)\theta} + \sum_{n=1}^{\infty} T_n\mathrm{e}^{-\mathrm{i}(n+3)\theta} + \sum_{n=1}^{\infty} U_n\mathrm{e}^{\mathrm{i}(n+4)\theta} + \sum_{n=1}^{\infty} V_n\mathrm{e}^{-\mathrm{i}(n+4)\theta}\Big].
\end{aligned} \tag{52}$$

By equating the coefficients of $\mathrm{e}^{\mathrm{i}n\theta}$ in Eq. (52), the relationships between the unknown coefficients can be obtained. This yields a sufficient number of equations to solve for the unknown coefficients. Depending on the level of accuracy required, different values of J and the number of the coefficients in the power series, i.e., n, are chosen.

3. Numerical results and discussion

In this section, selected numerical results for the plane strain case are presented without loss of any generality. For plane strain case, the surface/interface effects are represented by the parameters τ^0 and K^S (or τ^0, Λ_1 and Λ_6, see Appendix A). Experiments have been performed to determine the surface stress which has an order of 1 N/m (Ruud et al., 1993; Josell et al., 1999). The embedded atom method was used by Miller and Shenoy (2000) and Shenoy (2005) to determine the surface elastic constants. Their results indicated that the surface elastic constants depend on the material type and the surface crystal orientation. For example, for *Al* [1 0 0] surface: $\lambda^S = 3.4939$ N/m, $\mu^S = -5.4251$ N/m, $\tau^0 = 0.5689$ N/m, $K^S = -7.9253$ N/m; while for *Al* [1 1 1] surface: $\lambda^S = 6.8511$ N/m, $\mu^S = -0.3760$ N/m, $\tau^0 = 0.9108$ N/m, $K^S = 5.1882$ N/m (Miller and Shenoy, 2000). In the ensuing numerical results, unless specified otherwise, $\tau^0 = \pm 1$ N/m and $K^S = 5.19, -7.92, \pm 10$ N/m. Note that negative K^S values are realistic based on atomistic calculations.

The number of the terms in the infinite series representation of the complex potential functions is chosen so that the error in the numerical calculation is maintained below 1%. This is achieved by increasing the number of terms in the series representation until the difference between two consecutive sums is less than 1%. Accuracy of the numerical calculations is checked by setting the surface elastic constants and residual surface stress to negligibly small values and comparing the resulting numerical solutions with the classical elasticity solution for an elliptic hole in an infinite plane subjected to remote uniaxial tension. It is found that the two solutions agree very closely.

3.1. Infinite plane with an elliptical hole

An infinite plane of aluminum containing an elliptical hole under far-field loading is considered. The bulk elastic constants for aluminum are: $\lambda_M = 58.17$ GPa, $\mu_M = 26.13$ GPa (Meyers and Chawla, 1999). The effect

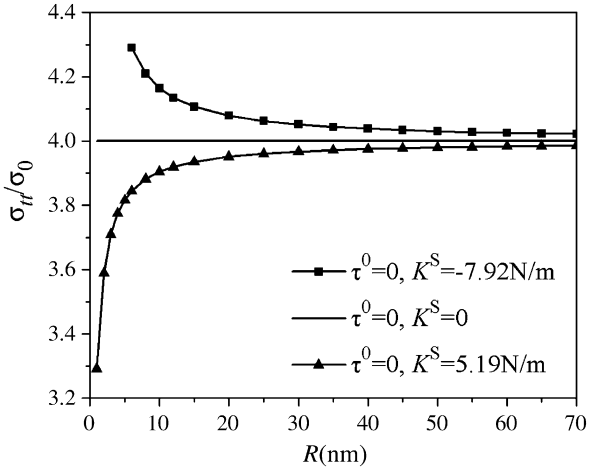

Fig. 3. Variation of stress concentration factor at $\theta = 0$ with hole size R and K^S ($a/b = 1.5$) under uniaxial loading $\sigma_{yy}^{\infty} = \sigma_0$.

of the surface elastic constant, $K^S = 2\,\mu^S + \lambda^S - \tau^0$, is first studied by setting $\tau^0 = 0$. In this case, the stress concentration factor at $\theta = 0$, σ_{tt}/σ_0, is independent of the magnitude of the applied loading. Fig. 3 shows the stress concentration factor for various hole sizes $R[= (a + b)/2]$ under uniaxial loading with $a/b = 1.5$. As expected the classical solution in which $\tau^0 = 0$ and $K^S = 0$ is independent of the hole size, while the surface stress effects cause the stress concentration to be size-dependent especially when R is less than 20 nm. The stress concentration factor increases or decreases when $K^S < 0$ or $K^S > 0$. The surface stress effects are negligible when R is over 40 nm and the stress concentration factor is equal to the classical elasticity solution. This behavior is similar to that of the circular case (Tian and Rajapakse, 2007) and of the spherical case (Sharma et al., 2003). However, for $K^S < 0$, hoop stress is found to become highly oscillatory and singular at some values for R less than 6 nm. Such unstable behaviour is not noted for $K^S > 0$ in which case the stress becomes smaller as R decreases.

It is proposed to further investigate this phenomenon by considering the case of a circular hole under uniaxial or biaxial loading. Closed-form analytical solution for the plane strain case is (Tian and Rajapakse, 2007)

$$\frac{\sigma_{\theta\theta}}{\sigma_0} = \frac{1+\Delta}{2} + \frac{1-\Delta}{2}\cos 2\theta - \frac{\frac{1}{2}(\Lambda_1\Lambda_2 - 1)(1+\Delta) + \tau^0/\sigma_0 R_0}{1+2\Lambda_1} - \frac{\frac{3}{2}(\Lambda_1\Lambda_2 - 1)(1-\Delta)}{1+4\Lambda_1+\Lambda_1\Lambda_2}\cos 2\theta, \tag{53}$$

$$\frac{\sigma_{rr}}{\sigma_0} = \frac{1+\Delta}{2} - \frac{\frac{1}{2}(\Lambda_1\Lambda_2 - 1)(1+\Delta) + \tau^0/\sigma_0 R_0}{1+2\Lambda_1} + \frac{(\Lambda_1\Lambda_2 + 2\Lambda_1)(1-\Delta)}{1+4\Lambda_1+\Lambda_1\Lambda_2}\cos 2\theta, \tag{54}$$

$$\frac{u_r}{\sigma_0 R_0/\mu_M} = \frac{(\kappa_M+1)(1+\Delta)}{8} - \frac{\frac{1}{2}(\Lambda_1\Lambda_2 - 1)(1+\Delta) + \tau^0/\sigma_0 R_0}{2(1+2\Lambda_1)} - \frac{(1-\Delta)}{4}\cos 2\theta - \frac{\frac{1}{4}(\kappa_M+1)(1+2\Lambda_1)(1-\Delta)}{1+4\Lambda_1+\Lambda_1\Lambda_2}\cos 2\theta - \frac{\frac{1}{4}(\Lambda_1\Lambda_2 - 1)(1-\Delta)}{1+4\Lambda_1+\Lambda_1\Lambda_2}\cos 2\theta, \tag{55}$$

$$\frac{u_\theta}{\sigma_0 R_0/\mu_M} = \frac{1-\Delta}{4}\sin 2\theta - \frac{\frac{1}{4}(1-\kappa_M)(1-\Delta)(1+2\Lambda_1)}{1+4\Lambda_1+\Lambda_1\Lambda_2}\sin 2\theta - \frac{\frac{1}{4}(\Lambda_1\Lambda_2 - 1)(1-\Delta)}{1+4\Lambda_1+\Lambda_1\Lambda_2}\sin 2\theta. \tag{56}$$

Here, σ_0 is the applied loading magnitude, R_0 is the radius of the circular hole and $\Delta = 0$ for uniaxial loading and $\Delta = 1$ for biaxial loading. Note that when $K^S < 0$, Λ_1 is negative. Therefore, the denominators containing Λ_1 in Eqs. (53)–(56) can be zero for certain radii resulting in singular stress and displacement fields. The corresponding radii are very small, less than 1 nm, for the values of K^S corresponding to aluminum. A similar phenomenon exist for the elliptical case, however, there appear to be many hole sizes R which induce singular stresses. Some of these R values can be relatively large (>5 nm) depending on the geometry of the ellipse, surface elastic constant K^S and elastic properties of the matrix material.

The authors developed a finite element scheme based on Gurtin–Murdoch theory to further compare with the current numerical solutions. Details are not presented here for brevity but the finite element solutions also show unstable regions for negative K^S values. Following Murdoch (1976), the surface elasticity tensor is positive semi-definite. This is in contrast to the bulk elasticity tensor which is positive definite. The uniqueness of the solution is related to the condition of positive definiteness of total energy (i.e., bulk and surface) as surfaces cannot exist alone. The finite element simulations show that total stiffness matrix remains positive definite for negative K^S until the inhomogeneity dimensions reduce below some critical values. Thereafter, the total stiffness for negative K^S could become non-positive definite because the stiffness contribution associated with the surface elasticity tends to dominate over that due to bulk elasticity. This results in ill-conditioning of the stiffness matrix and unstable solutions for some inhomogeneity dimensions as in Fig. 3. Note that for $R > 30$ nm (Fig. 3), the surface energy effects are negligible for any K^S value and the solution is very close to the classical solution based only on bulk elasticity. The theoretical basis for the unstable behaviour of the solution for negative K^S is therefore the positive semi-definite nature of the surface elasticity tensor. Some issues related to surface energy at the nanoscale were recently discussed by Lodziana et al. (2004) and Mathur et al. (2005). The present model does not include plastic properties and other non-linearities of nanoscale materials which can also affect the response of a nanoscale structure.

Fig. 4 shows the stress concentration factor for various hole sizes R with $a/b = 3$ under uniaxial loading. The result is similar to the case of $a/b = 1.5$. However, the effect of the surface elastic constants K^S is more significant. Stress concentration shows high size-dependency when R is less than 40 nm. The difference between the classical and the current results can reach over 20% when $R = 2$ nm for $K^S > 0$. Tangential stress for $K^S < 0$ is unstable below 15 nm. It is noted that the results are similar for other values of a/b, and as the value of a/b increases, the effect of the surface elastic constant K^S becomes more pronounced and the value of R below which the stress becomes unstable when $K^S < 0$ increases.

Fig. 5 shows the variation of normalized tangential stress $[\sigma_{tt}(R,\theta)/\sigma_0]$ along the surface of a hole with $a/b = 1.5$ and $R = 6$ nm under uniaxial loading when $\tau^0 = 0$. For positive value of K^S, the normalized stress is reduced at $\theta = 0$ and increased at $\theta = \pi/2$ when compared to the classical result. Opposite behavior can be seen for negative value of K^S. Fig. 6 shows the variation of stresses σ_{22} and σ_{11} along the positive x_1-direction. The surface stress effect is significant only near the hole surface but diminishes quite rapidly as x_1 increases especially in the case of σ_{22}. Fig. 6b shows that, when compared to the classical solution, the normalized stress σ_{11}/σ_0 is higher near the hole surface but slightly smaller far from the hole for positive values of K^S. Opposite behavior is noted for negative values of K^S. Similar behavior of stresses along the hole surface and x_1-direction is observed for other values of a/b as well.

Consider next the influence of residual surface stress τ^0 on a plane containing an elliptical hole by setting $K^S = 0$ (or $\Lambda_1 = 0$). The numerical solutions for stress do not show any instability problem with respect to τ^0.

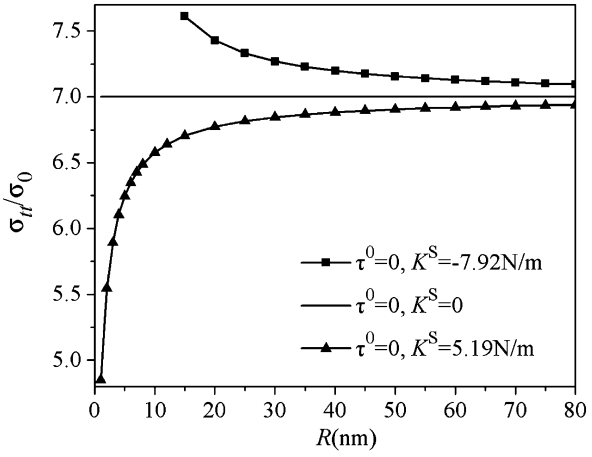

Fig. 4. Variation of stress concentration factor at $\theta = 0$ with the hole size R and K^S ($a/b = 3$) under uniaxial loading $\sigma^{\infty}_{yy} = \sigma_0$.

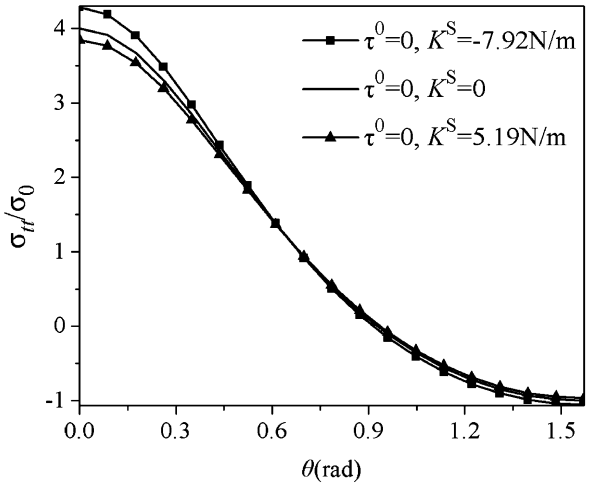

Fig. 5. Variation of stress σ_{11} along hole surface under uniaxial loading $\sigma_{yy}^{\infty} = \sigma_0$ ($a/b = 1.5$, $R = 6$ nm).

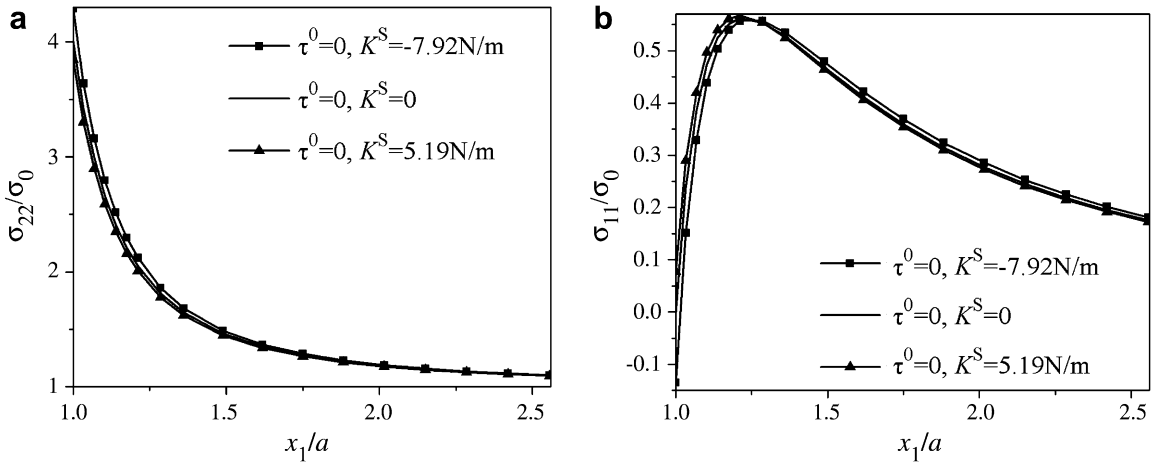

Fig. 6. Variation of stresses σ_{22} and σ_{11} along the x_1-direction for different K^S under uniaxial loading $\sigma_{yy}^{\infty} = \sigma_0$ ($a/b = 1.5$, $R = 6$ nm). (a) Variation of stresses σ_{22}. (b) Variation of stresses σ_{11}.

This behaviour can be easily confirmed from Eq. (53) for the circular case as the denominators cannot be equal to zero. To show the effect of τ^0, let σ_{22}^C and σ_{11}^C denote the stress components corresponding to the classical elasticity solution, respectively, and let σ_{22}^S and σ_{11}^S denote the stress components due to the residual surface stress τ^0. Fig. 7 shows the variation of σ_{22}^C and σ_{11}^C normalized by σ_0 and σ_{22}^S and σ_{11}^S normalized by τ^0/R along the positive x_1-direction under uniaxial loading when $a/b = 1.5$. The residual surface stress shows a significant influence on stress field only in the vicinity of the hole surface. Its effect is negligible at a distant greater than four times the major semi-axis. Note that normalized stress components due to τ^0 shown in Fig. 7 are independent of R.

3.2. Infinite plane with an elliptical inhomogeneity

Nanoscale inhomogeneities are found in modern developments such as quantum dots and nano-composites. To show the surface/interface effect on the elastic field, a matrix–inhomogeneity system made out of

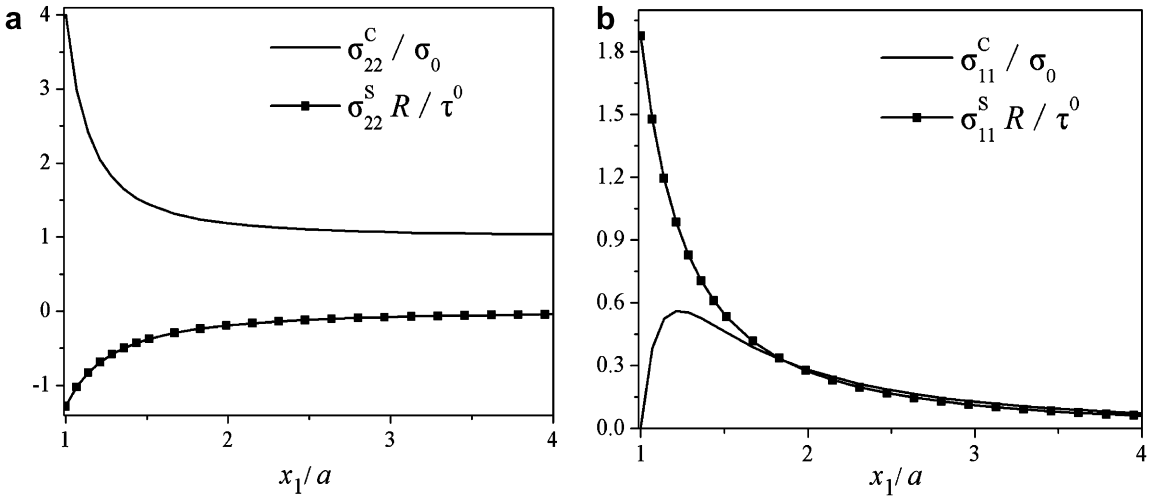

Fig. 7. Variation of stress components of σ_{22} and σ_{11} along the x_1-direction for a hole with residual surface stress under uniaxial loading $\sigma_{yy}^{\infty} = \sigma_0 (a/b = 1.5, \tau^0 \neq 0)$. (a) Variation of stresses σ_{22}. (b) Variation of stresses σ_{11}.

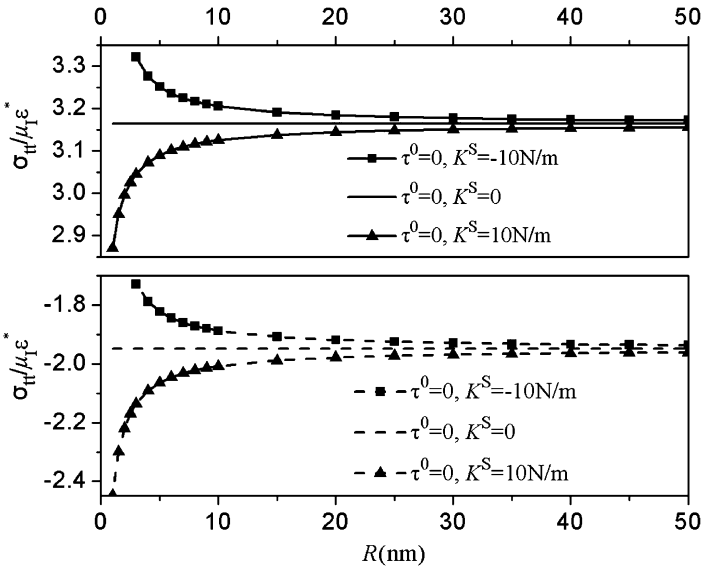

Fig. 8. Variation of normalized stress at $\theta = 0$ on the interface with the inhomogeneity size R and $K^S(a/b = 1.5)$ under a uniform dilatational eigenstrain ε^* (solid line for matrix and dash line for inhomogeneity).

InAs/GaAs is considered. The bulk elastic constants used are: $\lambda_I = 50.66$ GPa, $\mu_I = 19.0$ GPa for InAs, and $\lambda_M = 64.43$ GPa, $\mu_M = 32.9$ GPa for GaAs (Sharma and Ganti, 2002).

The influence of an eigenstrain, ε^*, in the inhomogeneity is now considered in the absence of far-field loading. Fig. 8 shows the normalized stress $\sigma_{tt}/\mu_I\varepsilon^*$ on the interface in the inhomogeneity and the matrix for various values of R for $a/b = 1.5$. The size-dependent behaviour of the stress field is evident for an inhomogeneity with R smaller than 15 nm. The effect of K^S is slightly more pronounced in the inhomogeneity than in the matrix and stress becomes unstable for $K^S < 0$ when R is below 3 nm.

Now consider Eshelby's problem in the presence of surface/interface effects. Eshelby (1957) obtained a uniform elastic field for an ellipsoidal inhomogeneity under a uniform eigenstrain in the classical case. As shown in Fig. 9, the non-dimensional normal strains in the x_1-direction and x_2-direction are no longer uniform and vary along the interface (in the inhomogeneity, $\varepsilon = \varepsilon^e + \varepsilon^*$, where ε is the actual strain and ε^e is the elastic

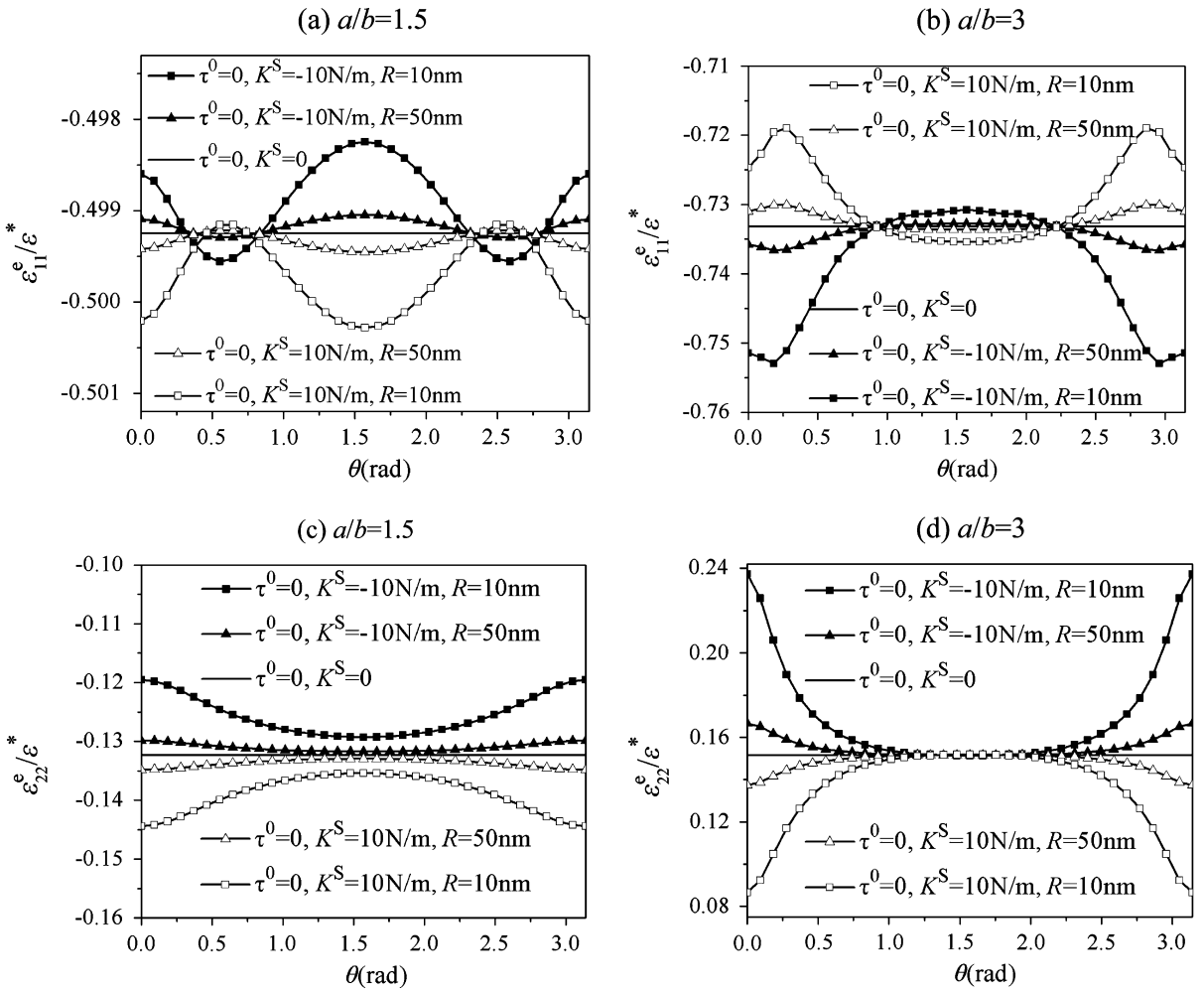

Fig. 9. Variation of normalized strain along the interface of an inhomogeneity for different values of K^S and R under a uniform dilatational eigenstrain.

strain). As the inhomogeneity becomes smaller (e.g., $R = 10$ nm), the effects of K^S and the non-uniformity of the elastic field are more prominent. The non-uniformity of strain field is more obvious as a/b increases and more surface stress effects can be observed for ε^e_{22} than ε^e_{11}. Similar behavior is observed for shear strain. Eshelby tensor is therefore size-dependent and non-uniform for an elliptical inhomogeneity, which is consistent with the conclusion pointed out by Sharma and Ganti (2004) for an inhomogeneity with non-constant curvature.

4. Summary and conclusion

In this paper, elastic state of an infinite matrix with a nanoscale elliptical inhomogeneity under arbitrary remote loading or a uniform eigenstrain in the inhomogeneity is studied. The formulation is based on the Gurtin–Murdoch surface/interface elasticity model and the complex potential function method of Muskhelishvili for plane elasticity problems. The analytic potential functions, which are expressed by infinite power series, can only be obtained approximately. The numerical results show that the elastic state is size-dependent when the inhomogeneity dimensions are below 50 nm. Stress concentration can be decreased or increased due to the local hardening/softening around the surface/interface depending on whether the surface elastic constant parameter K^S is positive or negative. The

solutions for stresses show unstable behaviour below a certain value of R when the surface elastic constant K^S is negative. This behaviour is related to the positive semi-definite nature of the surface elasticity tensor. The effect of the residual surface/interface stress also depends on the size of the hole/inhomogeneity but the resulting stress field shows no instability. Eshelby tensor for a uniform eigenstrain is size-dependent and no longer uniform in the presence of surface/interface stresses. The present solution is a benchmark solution that can be used in the verification of accuracy of numerical methods for the present class of problems and study of effective properties of nano-composites.

Acknowledgment

The work presented in this paper was supported by a research grant from the Natural Sciences and Engineering Research Council of Canada.

Appendix A

Using the expression for the curvature $\frac{1}{R_0}=\frac{(1-m^2)/R}{|m'(\xi)/R|^3}$ (see Appendix B) and Eq. (16), the interface stress in the matrix can be expressed as

$$\left(\frac{\frac{1}{2}\sigma^{\mathrm{S}}_{tt}}{R_0}\right)_{\mathrm{M}} m'(\xi)\overline{m'(\xi)}/R=\frac{(1-m^2)}{|m'(\xi)/R|^3}\left[\frac{\frac{1}{2}\tau^0 m'(\xi)\overline{m'(\xi)}}{R^2}+\Lambda_1\left(\frac{\Theta_{\mathrm{M}}(\xi)\xi^2}{R}+\frac{\overline{\Theta_{\mathrm{M}}(\xi)\xi^2}}{R}\right)\right.$$
$$\left.+(\Lambda_1+\Lambda_4)\Lambda_2\left(\frac{\phi'_{\mathrm{M}}(\xi)m'(\xi)}{R}+\frac{\overline{\phi'_{\mathrm{M}}(\xi)m'(\xi)}}{R}\right)\right]\Bigg\},\ \text{on } \Gamma, \tag{A1}$$

where

$$\Lambda_1=\frac{K^{\mathrm{S}}}{8\mu_{\mathrm{M}}R},\quad K^S=2\mu^S+\lambda^S-\tau^0,\quad \Lambda_2=\frac{2\mu_{\mathrm{M}}}{Q_{\mathrm{M}}},\quad \Lambda_4=\frac{\lambda^{\mathrm{S}}+\tau^0}{4\mu_{\mathrm{M}}R}\frac{v_{\mathrm{M}}}{v_{\mathrm{M}}-1}. \tag{A2}$$

By using Eqs. (16), (42) and (43), the derivative term in Eq. (45) is written as

$$\mathrm{i}\frac{\frac{1}{2}\partial(\sigma_{tt})_{\mathrm{M}}}{\partial t}m'(\xi)\overline{m'(\xi)}/R=\frac{1}{|m'(\xi)/R|^3}\left\{-\frac{\Lambda_1\Theta'_{\mathrm{M}}(\xi)}{R}[-m\xi+(1+m^2)\xi^3-m\xi^5]-\frac{\Lambda_1\Theta_{\mathrm{M}}(\xi)}{R}\right.$$
$$\times[2(1+m^2)\xi^2-4m]+\frac{\Lambda_1\overline{\Theta'_{\mathrm{M}}(\xi)}}{R}[-m\xi^{-5}+(1+m^2)\xi^{-3}-m\xi^{-1}]$$
$$+\frac{\Lambda_1\overline{\Theta_{\mathrm{M}}(\xi)}}{R}[2(1+m^2)\xi^{-2}-4m]-\Lambda_2(\Lambda_1+\Lambda_4)$$
$$\times\left[\frac{\phi''_{\mathrm{M}}(\xi)m'(\xi)}{R}-\frac{\phi'_{\mathrm{M}}(\xi)m''(\xi)}{R}\right]\frac{(\overline{m'(\xi)})^2\xi}{R^2}+\Lambda_2(\Lambda_1+\Lambda_4)$$
$$\left.\times\left[\frac{\overline{\phi''_{\mathrm{M}}(\xi)m'(\xi)}}{R}-\frac{\overline{\phi'_{\mathrm{M}}(\xi)m''(\xi)}}{R}\right]\frac{(m'(\xi))^2\overline{\xi}}{R^2}\right\},\quad \text{on } \Gamma. \tag{A3}$$

In the inhomogeneity, considering the effect of eigenstrain, the actual strain is regarded as the sum of elastic strain and eigenstrain. However, the calculation is the same as that in the matrix and the result is similar. In Eqs. (A1), (A2), (A3), ϕ_{M} and Θ_{M} are replaced by ϕ_{I} and Θ_{I}, respectively; Λ_1 and Λ_2 by Λ_6 and Λ_7, respectively; Λ_4 by Λ_5; τ^0 by $\tau^0+8(\Lambda_6+\Lambda_5)\mu_{\mathrm{I}}\,R\varepsilon^*$, and others keep the same. Here

$$\Lambda_5=\frac{\lambda^{\mathrm{S}}+\tau^0}{4\mu_{\mathrm{I}}R}\frac{v_{\mathrm{I}}}{v_{\mathrm{I}}-1},\quad \Lambda_6=\frac{K^{\mathrm{S}}}{8\mu_{\mathrm{I}}R},\quad \Lambda_7=\frac{2\mu_{\mathrm{I}}}{Q_{\mathrm{I}}}. \tag{A4}$$

Multiplying Eq. (45) by a factor $\frac{m'(\xi)\overline{m'(\xi)}/R}{m'(\xi)/R}$ and using Eqs. (24), (25), (31), (32), (A1) and (A3) yields

$$\begin{aligned}\frac{m'(\xi)\overline{m'(\xi)}/R}{m'(\xi)/R}\left[\frac{\sigma_{tt}^{S}}{R_0}+\mathrm{i}\frac{\partial\sigma_{tt}^{S}}{\partial t}\right] &= \frac{1}{m'(\xi)/R}\frac{1}{|m'(\xi)/R|^3}[g_0+h_0+(g_1+h_1)\mathrm{e}^{-\mathrm{i}\theta}+(g_2+h_2)\mathrm{e}^{\mathrm{i}\theta}+(g_3+h_3)\mathrm{e}^{-2\mathrm{i}\theta}\\ &\quad+(g_4+h_4)\mathrm{e}^{2\mathrm{i}\theta}+(g_5+h_5)\mathrm{e}^{-3\mathrm{i}\theta}+(g_6+h_6)\mathrm{e}^{3\mathrm{i}\theta}+h_7\mathrm{e}^{-4\mathrm{i}\theta}+h_8\mathrm{e}^{4\mathrm{i}\theta}\\ &\quad+\sum_{n=1}^{\infty}S_n\mathrm{e}^{\mathrm{i}(n+3)\theta}+\sum_{n=1}^{\infty}T_n\mathrm{e}^{-\mathrm{i}(n+3)\theta}+\sum_{n=1}^{\infty}U_n\mathrm{e}^{\mathrm{i}(n+4)\theta}+\sum_{n=1}^{\infty}V_n\mathrm{e}^{-\mathrm{i}(n+4)\theta}],\quad \text{on } \Gamma,\end{aligned} \tag{A5}$$

where

$$\begin{aligned}g_0 &= \frac{1}{2}\tau^0(1-m^4)+\Lambda_2(\Lambda_1+\Lambda_4)(2-2m^2)A+4\Lambda_1 m(D_0-\overline{D}_0)\\ &\quad+\Lambda_2(\Lambda_1+\Lambda_4)[(5m-m^3)A_1+(-3m-m^3)\overline{A}_1]+12\Lambda_2(\Lambda_1+\Lambda_4)m^2(A_3+\overline{A}_3)\\ &\quad+\Lambda_1(1-m^2)(D_2+\overline{D}_2)+4\Lambda_1 m(-D_4+\overline{D}_4),\\ g_1 &= 14\Lambda_2(\Lambda_1+\Lambda_4)mA_2+6\Lambda_2(\Lambda_1+\Lambda_4)m^2\overline{A}_2-20\Lambda_2(\Lambda_1+\Lambda_4)m^2A_4\\ &\quad+2\Lambda_1 D_3+3\Lambda_1 m\overline{D}_3-5\Lambda_1 mD_5,\\ g_2 &= -6\Lambda_2(\Lambda_1+\Lambda_4)m^2A_2+\Lambda_2(\Lambda_1+\Lambda_4)(-10m-4m^3)\overline{A}_2+20\Lambda_2(\Lambda_1+\Lambda_4)m^2\overline{A}_4\\ &\quad-3\Lambda_1 mD_3-2\Lambda_1 m^2\overline{D}_3+5\Lambda_1 m\overline{D}_5,\\ g_3 &= -\frac{1}{2}\tau^0 m(1-m^2)+\Lambda_2(\Lambda_1+\Lambda_4)(m-m^3)A+\Lambda_1(3+m^2)\overline{D}_0\\ &\quad+\Lambda_2(\Lambda_1+\Lambda_4)[(-3+m^2)A_1+2m^2\overline{A}_1+(27m+3m^3)A_3-30m^2A_5]\\ &\quad+2\Lambda_1 m(D_2+\overline{D}_2)+\Lambda_1(3+m^2)D_4-6\Lambda_1 mD_6,\\ g_4 &= -\frac{1}{2}\tau^0 m(1-m^2)+\Lambda_2(\Lambda_1+\Lambda_4)(3m^3-3m)A-\Lambda_1(1+3m^2)D_0\\ &\quad+\Lambda_2(\Lambda_1+\Lambda_4)[-2m^2A_1+(1+m^2)\overline{A}_1+(-21m-9m^3)\overline{A}_3+30m^2\overline{A}_5]\\ &\quad-2\Lambda_1 mD_2-2\Lambda_1 m\overline{D}_2+\Lambda_1(-1-3m^2)\overline{D}_4+6\Lambda_1 m\overline{D}_6,\\ g_5 &= \Lambda_2(\Lambda_1+\Lambda_4)[(-8-2m^2)A_2+(44m+8m^3)A_4-42m^2A_6]\\ &\quad+\Lambda_1 mD_3+\Lambda_1(4+2m^2)D_5-7\Lambda_1 mD_7,\\ g_6 &= \Lambda_2(\Lambda_1+\Lambda_4)[(4+6m^2)\overline{A}_2+(-36m-16m^3)\overline{A}_4+42m^2\overline{A}_6]\\ &\quad-\Lambda_1 m\overline{D}_3+\Lambda_1(-2-4m^2)\overline{D}_5+7\Lambda_1 m\overline{D}_7,\\ S_n &= \Lambda_2(\Lambda_1+\Lambda_4)[m(n-n^2)\overline{A}_n+(n+2)[n+2+(2n+3)m^2]\overline{A}_{n+2}]\\ &\quad+\Lambda_2(\Lambda_1+\Lambda_4)\{(n+4)[m+m^3-(n+5)(2m+m^3)]\overline{A}_{n+4}+(n+6)(n+7)m^2\overline{A}_{n+6}\}\\ &\quad+\Lambda_1(n-1)m\overline{D}_{n+3}+\Lambda_1[3+m^2-(n+5)(1+m^2)]\overline{D}_{n+5}+\Lambda_1(n+7)m\overline{D}_{n+7},\\ T_n &= \Lambda_2(\Lambda_1+\Lambda_4)[(n^2-n)mA_n-(n+2)(2nm^2+m^2+n+4)A_{n+2}]\\ &\quad+\Lambda_2(\Lambda_1+\Lambda_4)[(n+4)(nm^3+2m^3+2nm+11m)A_{n+4}-(n+6)(n+7)m^2A_{n+6}]\\ &\quad+\Lambda_1(1-n)mD_{n+3}+\Lambda_1[(n+5)(1+m^2)-(1+3m^2)]D_{n+5}-\Lambda_1(n+7)mD_{n+7},\end{aligned} \tag{A6}$$

$$
\begin{aligned}
h_0 &= \frac{1}{2}[\tau^0 + 8(\Lambda_5+\Lambda_6)\mu_1 R\varepsilon^*](1-m^4) + \Lambda_6[4m(O_0-\overline{O}_0) + (1-m^2)(P_2+\overline{P}_2) + 4m(\overline{P}_4 - P_4)] \\
&\quad + \Lambda_7(\Lambda_5+\Lambda_6)[(1-5m^2)E_1 + (1+3m^2)\overline{E}_1 + 12m(E_3-\overline{E}_3)] \\
&\quad + \Lambda_7(\Lambda_5+\Lambda_6)[(5m-m^3)F_1 + (-3m-m^3)\overline{F}_1 + 12m^2(\overline{F}_3 - F_3)], \\
h_1 &= -5\Lambda_6 m\overline{O}_1 + 3\Lambda_6 mP_1 + 2\Lambda_6\overline{P}_1 + 2\Lambda_6 P_3 + 3\Lambda_6 m\overline{P}_3 - 5\Lambda_6 mP_5 \\
&\quad + \Lambda_7(\Lambda_5+\Lambda_6)[6mE_2 + (4+10m^2)\overline{E}_2 - 20m\overline{E}_4] \\
&\quad + \Lambda_7(\Lambda_5+\Lambda_6)(14mF_2 + 6m^2\overline{F}_2 - 20m^2F_4), \\
h_2 &= 5\Lambda_6 mO_1 - 2\Lambda_6 m^2P_1 - 3\Lambda_6 m\overline{P}_1 - 3\Lambda_6 mP_3 - 2\Lambda_6 m^2\overline{P}_3 + 5\Lambda_6 m\overline{P}_5 \\
&\quad - \Lambda_7(\Lambda_5+\Lambda_6)(14m^2E_2 + 6m\overline{E}_2 - 20mE_4) \\
&\quad + \Lambda_7(\Lambda_5+\Lambda_6)[-6m^2F_2 + (-10m-4m^3)\overline{F}_2 + 20m^2\overline{F}_4], \\
h_3 &= -\frac{1}{2}m(1-m^2)[\tau^0 + 8(\Lambda_6+\Lambda_5)\mu_1 R\varepsilon^*] + \Lambda_6(3+m^2)\overline{O}_0 - 6\Lambda_6 m\overline{O}_2 \\
&\quad + 2\Lambda_6 m(P_2+\overline{P}_2) + \Lambda_6(3+m^2)P_4 - 6\Lambda_6 mP_6 \\
&\quad + \Lambda_7(\Lambda_5+\Lambda_6)[2mE_1 - (m+m^3)\overline{E}_1 + (3+9m^2)\overline{E}_3 - 30m\overline{E}_5] \\
&\quad + \Lambda_7(\Lambda_5+\Lambda_6)[(-3+m^2)F_1 + 2m^2\overline{F}_1 + (27m+3m^3)F_3 - 30m^2F_5], \\
h_4 &= -\frac{1}{2}m(1-m^2)[\tau^0 + 8(\Lambda_6+\Lambda_5)\mu_1 R\varepsilon^*] - \Lambda_6(1+3m^2)O_0 + 6\Lambda_6 mO_2 \\
&\quad - 2\Lambda_6 m(P_2+\overline{P}_2) - \Lambda_6(1+3m^2)\overline{P}_4 + 6\Lambda_6 m\overline{P}_6 \\
&\quad + \Lambda_7(\Lambda_5+\Lambda_6)[(3m^3-m)E_1 - 2m\overline{E}_1 - (3+27m^2)E_3 + 30mE_5] \\
&\quad + \Lambda_7(\Lambda_5+\Lambda_6)[-2m^2F_1 + (1+m^2)\overline{F}_1 - (21m+9m^3)\overline{F}_3 + 30m^2\overline{F}_5], \\
h_5 &= \Lambda_6(4+2m^2)\overline{O}_1 - 7\Lambda_6 m\overline{O}_3 + \Lambda_6 m\overline{P}_1 + \Lambda_6 mP_3 + \Lambda_6(4+2m^2)P_5 - 7\Lambda_6 mP_7 \\
&\quad - \Lambda_7(\Lambda_5+\Lambda_6)[(6m+4m^3)\overline{E}_2 - (16+36m^2)\overline{E}_4 + 42m\overline{E}_6] \\
&\quad + \Lambda_7(\Lambda_5+\Lambda_6)[(-8+2m^2)F_2 + (44m+8m^3)F_4 - 42m^2F_6], \\
h_6 &= -\Lambda_6(2+4m^2)O_1 + 7\Lambda_6 mO_3 - \Lambda_6 mP_1 - \Lambda_6 m\overline{P}_3 - \Lambda_6(2+4m^2)\overline{P}_5 + 7\Lambda_6 m\overline{P}_7 \\
&\quad + \Lambda_7(\Lambda_6+\Lambda_5)[(2m+8m^3)E_2 - (8+44m^2)E_4 + 42mE_6] \\
&\quad + \Lambda_7(\Lambda_6+\Lambda_5)[(4+6m^2)\overline{F}_2 - (36m+16m^3)\overline{F}_4 + 42m^2\overline{F}_6], \\
h_7 &= \Lambda_6(5+3m^2)\overline{O}_2 - 8\Lambda_6 m\overline{O}_4 + \Lambda_6(5+3m^2)P_6 - 8\Lambda_6 mP_8 \\
&\quad + \Lambda_7(\Lambda_6+\Lambda_5)[-(15m+9m^3)\overline{E}_3 + (25+55m^2)\overline{E}_5 - 56m\overline{E}_7] \\
&\quad + \Lambda_7(\Lambda_6+\Lambda_5)[-(15+9m^2)F_3 + (65m+15m^3)F_5 - 56m^2F_7], \\
h_8 &= -\Lambda_6(3+5m^2)O_2 + 8\Lambda_6 mO_4 - \Lambda_6(3+5m^2)\overline{P}_6 + 8\Lambda_6 m\overline{P}_8 \\
&\quad + \Lambda_7(\Lambda_6+\Lambda_5)[(9m+15m^3)E_3 - (15+65m^2)E_5 + 56mE_7] \\
&\quad + \Lambda_7(\Lambda_6+\Lambda_5)[(9+15m^2)\overline{F}_3 - (55m+25m^3)\overline{F}_5 + 56m^2\overline{F}_7], \\
U_n &= n\Lambda_6 mO_n - \Lambda_6[n+3+(n+5)m^2]O_{n+2} + (n+8)\Lambda_6 mO_{n+4} \\
&\quad + n\Lambda_6 m\overline{P}_{n+4} - \Lambda_6[n+3+(n+5)m^2]\overline{P}_{n+6} - (n+8)\Lambda_6 m\overline{P}_{n+8} \\
&\quad - n(n+1)\Lambda_7(\Lambda_6+\Lambda_5)m^2E_{n+1} + \Lambda_7(\Lambda_6+\Lambda_5)(n+3)[(2n+3)m + (n+5)m^2]E_{n+3} \\
&\quad - \Lambda_7(\Lambda_6+\Lambda_5)(n+5)[n+3+(2n+13)m^2]E_{n+5} + (n+7)(n+8)\Lambda_7(\Lambda_6+\Lambda_5)mE_{n+7} \\
&\quad - n(n+1)\Lambda_7(\Lambda_6+\Lambda_5)m\overline{F}_{n+1} + \Lambda_7(\Lambda_6+\Lambda_5)(n+3)[n+3+(2n+5)m^2]\overline{F}_{n+3} \\
&\quad + \Lambda_7(\Lambda_6+\Lambda_5)\{-(n+5)\big[(2n+11)m + (n+5)m^3\big]\overline{F}_{n+5} + (n+7)(n+8)m^2\overline{F}_{n+7}\}, \\
V_n &= -n\Lambda_6 m\overline{O}_n + \Lambda_6[n+3+(n+3)m^2]\overline{O}_{n+2} - (n+8)\Lambda_6 m\overline{O}_{n+4} \\
&\quad - n\Lambda_6 mP_{n+4} + \Lambda_6[n+5+(n+3)m^2]P_{n+6} - (n+8)\Lambda_6 mP_{n+8} \\
&\quad + n(n+1)\Lambda_7(\Lambda_6+\Lambda_5)m^2\overline{E}_{n+1} - \Lambda_7(\Lambda_6+\Lambda_5)(n+3)[(2n+5)m + (n+3)m^2]\overline{E}_{n+3} \\
&\quad - \Lambda_7(\Lambda_6+\Lambda_5)(n+5)[n+5+(2n+11)m^2]\overline{E}_{n+5} - (n+7)(n+8)\Lambda_7(\Lambda_6+\Lambda_5)m\overline{E}_{n+7} \\
&\quad + n(n+1)\Lambda_7(\Lambda_6+\Lambda_5)mF_{n+1} - \Lambda_7(\Lambda_6+\Lambda_5)(n+3)[n+5+(2n+3)m^2]F_{n+3} \\
&\quad + \Lambda_7(\Lambda_6+\Lambda_5)\{(n+5)\big[(2n+13)m + (n+3)m^3\big]F_{n+5} - (n+7)(n+8)m^2F_{n+7}\}.
\end{aligned}
\tag{A7}
$$

Appendix B

Curvature of the ellipse

In the (x_1, x_2)-coordinate system, the equation of ellipse is

$$\frac{x_1^2}{a^2}+\frac{x_2^2}{b^2}=1. \tag{B1}$$

Note that the variable x_2 can be written as a function of x_1 based on Eq. (B1) and

$$x_1=\frac{z+\bar{z}}{2},\quad x_2=\frac{z-\bar{z}}{2i},\quad z=R\left(\xi+\frac{m}{\xi}\right), \tag{B2}$$

The curvature is expressed in terms of the complex variable ξ as follows:

$$\frac{1}{R_0}=\frac{|x_2''|}{(1+x_2'^2)^{3/2}}=\frac{(1-m^2)}{R}\frac{1}{|m'(\xi)/R|^3}. \tag{B3}$$

Infinite series representation of $(1+b^*\sin^2\theta)^{-3/2}$

Using the Fourier series in the complex form,

$$(1+b^*\sin^2\theta)^{-3/2}=I_0+\sum_{k=1}^{\infty}I_{2k}(\mathrm{e}^{\mathrm{i}2k\theta}+\mathrm{e}^{-\mathrm{i}2k\theta}), \tag{B4}$$

where

$$I_{2k}=\frac{1}{2\pi}\int_0^{2\pi}(1+b^*\sin^2\theta)^{-3/2}\cos(2k\theta)\,\mathrm{d}\theta. \tag{B5}$$

For a large integer k, the right-hand side of Eq. (B4) approaches a geometric series and this can be easily proved by a method similar to that used by Shen et al. (2000). Thus,

$$(1+b^*\sin^2\theta)^{-3/2}=I_0+\sum_{k=1}^{J-1}I_{2k}(\mathrm{e}^{\mathrm{i}2k\theta}+\mathrm{e}^{-\mathrm{i}2k\theta})+\sum_{k=0}^{\infty}I_{2(J+k)}[\mathrm{e}^{\mathrm{i}2(J+k)\theta}+\mathrm{e}^{-\mathrm{i}2(J+k)\theta}]. \tag{B6}$$

and consider the third term on the right-hand side as a geometric series for large integer J (approximately). Therefore,

$$\begin{aligned}\left(1+b^*\sin^2\theta\right)^{-3/2}\cong& I_0+\sum_{k=1}^{J-1}I_{2k}(\mathrm{e}^{\mathrm{i}2k\theta}+\mathrm{e}^{-\mathrm{i}2k\theta})+I_{2J}\left[\frac{\mathrm{e}^{\mathrm{i}2J\theta}}{1-m\mathrm{e}^{\mathrm{i}2\theta}}+\frac{\mathrm{e}^{-\mathrm{i}2J\theta}}{1-m\mathrm{e}^{-\mathrm{i}2\theta}}\right],\\ =&I_0+\sum_{k=1}^{J-1}I_{2k}(\mathrm{e}^{\mathrm{i}2k\theta}+\mathrm{e}^{-\mathrm{i}2k\theta})+I_{2J}\frac{\mathrm{e}^{\mathrm{i}2J\theta}+\mathrm{e}^{-\mathrm{i}2J\theta}-m[\mathrm{e}^{\mathrm{i}2(J-1)\theta}+\mathrm{e}^{\mathrm{i}2(1-J)\theta}]}{(1-m\mathrm{e}^{\mathrm{i}2\theta})(1-m\mathrm{e}^{-\mathrm{i}2\theta})}.\end{aligned} \tag{B7}$$

Power series expansion of $\frac{1}{m'(\xi)/R}\frac{1}{(1-m\mathrm{e}^{\mathrm{i}2\theta})(1-m\mathrm{e}^{-\mathrm{i}2\theta})}$

Consider the following equations ($|\xi|=1$)

$$\frac{1}{1-m\mathrm{e}^{\pm\mathrm{i}2\theta}}=\sum_{n=0}^{\infty}(m\mathrm{e}^{\pm\mathrm{i}2\theta})^n,\quad \frac{1}{m'(\xi)/R}=\frac{1}{1-m\mathrm{e}^{-\mathrm{i}2\theta}}=\sum_{n=0}^{\infty}(m\mathrm{e}^{-\mathrm{i}2\theta})^n. \tag{B8}$$

Therefore,

$$\frac{1}{m'(\xi)/R}\frac{1}{(1-m\mathrm{e}^{\mathrm{i}2\theta})(1-m\mathrm{e}^{-\mathrm{i}2\theta})}=\frac{1}{(1-m^2)^2}\left\{\sum_{n=1}^{\infty}\left[m^n+(1-m^2)nm^n\right]\mathrm{e}^{-\mathrm{i}2n\theta}+1+\sum_{n=1}^{\infty}\left(m\mathrm{e}^{\mathrm{i}2\theta}\right)^n\right\}. \tag{B9}$$

References

Cahn, J.W., Larché, F., 1982. Surface stress and chemical equilibrium of small crystals. II. Solid particles embedded in a solid matrix. Acta Metallurgica 30, 51–56.

Cammarata, R.C., 1994. Surface and interface stress effects in thin films. Progress in Surface Science 46, 1–38.

Cammarata, R.C., 1997. Surface and interface stress effects on interfacial and nanostructured materials. Materials Science and Engineering A 237, 180–184.

Cui, Y., Lieber, C.M., 2001. Functional nanoscale electronic devices assembled using silicon nanowire building blocks. Science 291, 851–853.

Duan, H.L., Wang, J., Huang, Z.P., Karihaloo, B.L., 2005. Size-dependent effective elastic constants of solids containing nano-inhomogeneities with interface stress. Journal of the Mechanics and Physics of Solids 53, 1574–1596.

England, A.H., 1971. Complex Variable Methods in Elasticity. Wiley-Interscience, London.

Eshelby, J.D., 1957. The determination of the elastic field of an ellipsoidal inclusion and related problems. Proceedings of the Royal Society A 241, 376–396.

Gibbs, J.W., 1906. The Scientific Papers of J. Willard Gibbs, vol I. Longmans Green, London.

Gurtin, M.E., Murdoch, A.I., 1975. A continuum theory of elastic material surfaces. Archive of Rational Mechanics and Analysis 57, 291–323.

Gurtin, M.E., Murdoch, A.I., 1978. Surface stress in solids. International Journal of Solids and Structure 14, 431–440.

Gurtin, M.E., Weissmuller, J., Larché, F., 1998. A general theory of curved deformable interfaces in solids at equilibrium. Philosophical Magazine A 78, 1093–1109.

Josell, D., Bonevich, J.E., Shao, J., Cammarata, R.C., 1999. Measuring the interface stress: silver/nickel interfaces. Journal of Materials Research 14, 4358–4365.

Kuzumake, T., Miyazawa, K., Ichinose, H., Ito, K., 1998. Processing of carbon nanotube reinforced aluminum composite. Journal of Materials Research 13, 2445–2449.

Lodziana, Z., Topsoe, N., Norskov, J.K., 2004. A negative surface energy for alumina. Nature Materials 3, 289–293.

Mathur, A., Sharma, P., Cammarata, R.C., 2005. Negative surface energy – clearing up confusion. Nature Materials 4, 186.

Meyers, M.A., Chawla, K.K., 1999. Mechanical Behavior of Materials. Prentice Hall, Englewood Cliffs, NJ, pp. 92.

Miller, R.E., Shenoy, V.B., 2000. Size-dependent elastic properties of nanosized structural elements. Nanotechnology 11, 139–147.

Murdoch, A.I., 1976. A thermodynamical theory of elastic material interfaces. Quarterly Journal of Mechanics and Applied Mathematics 29, 245–275.

Muskhelishvili, N.I., 1963. Some Basic Problems of the Mathematical Theory of Elasticity. P. Noodhoff Ltd., Groningen, The Netherlands.

Naganuma, T., Kagawa, Y., 2002. Effect of particle size on the optically transparent nano meter-order glass particle-dispersed epoxy matrix composites. Composites Science and Technology 62, 1187–1189.

Nix, W.D., Gao, H., 1998. An atomistic interpretation of interface stress. Scripta Materialia 39, 1653–1661.

Poncharal, P., Wang, Z., Ugarte, D., de Heer, W.A., 1999. Electrostatic deflections and electromechanical resonances of carbon nanotubes. Science 283, 1513–1516.

Povstenko, Y.Z., 1993. Theoretical investigation of phenomena caused by heterogeneous surface tension in solids. Journal of the Mechanics and Physics of Solids 41, 1499–1514.

Ruud, J.A., Witvrouw, A., Spaepen, F., 1993. Bulk and interface stresses in silver–nickel multilayered thin films. Journal of Applied Physics 74, 2517–2523.

Sharma, P., Ganti, S., 2002. Interfacial elasticity corrections to size-dependent strain-state of embedded quantum dots. Physica Status Solidi B 234, R10–R12.

Sharma, P., Ganti, S., Bhate, N., 2003. Effect of surfaces on the size-dependent elastic state of nano-inhomogeneities. Applied Physics Letters 82, 535–537.

Sharma, P., Ganti, S., 2004. Size-dependent Eshelby's tensor for embedded nano-inclusions incorporating surface/interface energies. ASME Journal of Applied Mechanics 71, 663–671.

Shen, H., Schiavone, P., Ru, C.Q., Mioduchowski, A., 2000. An elliptic inclusion with imperfect interface in anti-plane shear. International Journal of Solids and Structure 37, 4557–4575.

Shen, H., Schiavone, P., Ru, C.Q., Mioduchowski, A., 2001. Interfacial thermal stress analysis of an elliptical inclusion with a compliant interphase layer in plane elasticity. International Journal of Solids and Structure 38, 7587–7606.

Shenoy, V.B., 2005. Atomistic calculations of elastic properties of metallic fcc crystal surfaces. Physical Review B 71, 094104.

Stagni, L., 1991. Elastic field perturbation by an elliptic inhomogeneity with a sliding interface. Journal of Applied Mathematical Physics (ZAMP) 42, 811–820.

Tian, L., Rajapakse, R.K.N.D., 2007. Analytical solution for size-dependent elastic field of a nanoscale circular inhomogeneity. ASME Journal of Applied Mechanics 74, 568–574.

Wong, E., Sheehan, P.E., Lieber, C.M., 1997. Nanobeam mechanics: elasticity, strength and toughness of nanorods and nanotubes. Science 277, 1971–1975.